Tunable spatial heterogeneity in structure and composition within aqueous microfluidic droplets

Citation: Hui,Sophia Lee Su, Pengzhi Wang, Swee Kun Yap, T. Alan Hatton, and Saif A. Khan. Tunable Spatial Heterogeneity in Structure and Composition Within Aqueous Microfluidic Droplets. Biomicrofluidics 6, no. 2 (2012): 022005.

As Published: http://dx.doi.org/10.1063/1.3694841

Publisher: American Institute of Physics

Persistent URL: http://hdl.handle.net/1721.1/79363

Version: Author's final manuscript: final author's manuscript post peer review, without publisher's formatting or copy editing

Tunable spatial heterogeneity in structure and composition within aqueous microfluidic droplets

Su Hui Sophia Lee,[1] Pengzhi Wang,[2] Swee Kun Yap,[2] T. Alan Hatton,[1,3] and Saif A. Khan[1,2,a)]

[1]*Chemical and Pharmaceutical Engineering Programme, Singapore-MIT Alliance, National University of Singapore, Singapore 117576*
[2]*Department of Chemical and Biomolecular Engineering, National University of Singapore, 4 Engineering Drive 4, Singapore 117576*
[3]*Department of Chemical Engineering, Massachusetts Institute of Technology, Cambridge, Massachusetts 02139, USA*

(Received 2 December 2011; accepted 6 February 2012; published online 6 April 2012)

In this paper, we demonstrate biphasic microfluidic droplets with broadly tunable internal structures, from simple near-equilibrium drop-in-drop morphologies to complex yet uniform non-equilibrium steady-state structures. The droplets contain an aqueous mixture of poly(ethylene glycol) (PEG) and dextran and are dispensed into an immiscible oil in a microfluidic T-junction device. Above a certain well-defined threshold droplet speed, the inner dextran-rich phase is "stirred" within the outer PEG-rich phase. The stirred polymer mixture is observed to exhibit a near continuum of speed and composition-dependent phase morphologies. There is increasing interest in the use of such aqueous two-phase systems in microfluidic devices for biomolecular applications in a variety of contexts. Our work presents a method to go beyond equilibrium phase morphologies in generating microfluidic "multiple" emulsions and at the same time raises the possibility of biochemical experimentation in benign yet complex biomimetic milieus. © *2012 American Institute of Physics*. [http://dx.doi.org/10.1063/1.3694841]

I. INTRODUCTION

Aqueous two-phase systems (ATPS) are formed by mixing aqueous solutions of two incompatible polymers, such as poly(ethylene glycol) (PEG) and dextran (DEX), or one polymer and an appropriate salt, and consist of two equilibrium immiscible aqueous phases separated by a clear and stable interface.[1,2] Such systems have been of much scientific and technological interest due to several unique features that can be exploited for a wide variety of applications. For example, the low interfacial tension[3,4] and all-water environment in ATPS provides benign conditions, making them ideal for a broad range of biological applications such as extractive bioconversions[5] and separation of biomolecules.[2] Another promising application of much recent interest involves encapsulating ATPS in lipid vesicles to create experimental cell models for emulating complex reactions and pathways in living cells. The partitioning of the polymer mixtures into different thermodynamic phases within such encapsulated structures is analogous to micro-compartmentalization in living cells.[6]

Microfluidics-based applications of ATPS, such as fabrication of hydrogel beads,[7] nanolitre liquid patterning,[8] and separation of dyes,[1] cells,[9–13] and proteins[14,15] have been demonstrated in recent years. Several applications involve droplet-based microfluidics, and two typical droplet morphologies are used: "single emulsions" where one aqueous polymer droplet is dispersed in another aqueous polymer solution that serves as the continuous phase[1,7] or "double emulsions" where one aqueous polymer droplet is completely engulfed within another aqueous polymer

a)Author to whom correspondence should be addressed. Electronic mail: chesakk@nus.edu.sg. Tel.: (65) 6516 5133. Fax: (65) 6779 1936.

droplet, which is in turn dispersed in a third fluid that serves as a continuous phase.[13,16] We focus on the latter as the starting point in our work. Such "drop-in-drop" structures have also attracted significant interest in the context of aqueous-organic emulsification with capillary microfluidics,[17] and their internal structure can be understood by invoking well-established equilibrium criteria.[18]

In this paper, we demonstrate biphasic microfluidic droplets with broadly tunable internal structures beyond the simple, equilibrium drop-in-drop morphologies described above. These biphasic droplets exhibit complex, yet uniform, non-equilibrium steady-state structures. The droplets are composed of a phase-separating aqueous mixture of PEG and DEX and are dispensed into an immiscible oil at a microfluidic T-junction. In close analogy to lid-driven cavity models of immiscible fluid mixing,[19] above a certain well-defined threshold droplet speed, the inner dextran-rich phase is "stirred" within the outer PEG-rich phase. Such stirring of viscous, non-diffusing, immiscible fluid mixtures is common to natural and technological phenomena spanning an enormous range of length and time scales.[20,21] The stirred polymer mixture is observed to exhibit a near continuum of speed and composition-dependent phase morphologies. We map the influence of flow speed (U) and polymer composition (C_{PEG} and C_{DEX}) and construct a dynamic morphology map. Interestingly, the transitions between the different regions on the map can be understood by invoking models of droplet dynamics in unconfined linear Stokes flows.[22–26] Digital analysis of high-resolution droplet images also enables us to extract characteristic sizes of dispersed fluid elements, which we compare with estimates from models for immiscible fluid dispersions.[24,27] Complementary to existing droplet-based microfluidic methods in which complete and rapid homogenization of droplet contents is the norm,[28] our study presents a way to tune and control spatial heterogeneity within microfluidic droplets, thus paving the way for controlled chemical and biochemical experimentation within structured non-homogeneous environments.

II. MATERIALS AND METHODS

A. Materials

Octadecafluorodecahydronaphthalene (Sigma-Aldrich, mixture of cis and trans, 94%), 1H,1H,2H,2H-perfluoro-1-octanol (Sigma-Aldrich, 97%), dextran (from *Leuconostoc* spp., Sigma-Aldrich, Mr ~500 000), and poly(ethylene glycol) (Sigma-Aldrich, 40% (w/w) in water, average molecular weight ~8000) were used as obtained.

B. Microfluidic devices

Microfluidic devices were fabricated in polydimethylsiloxane (PDMS) using soft lithography.[29] Microchannel replicas were molded in PDMS (Sylgard 184 Silicone Elastomer Kit, Dow Corning) from master patterns fabricated using photolithography of a negative photoresist (SU-8 2050, MicroChem) on silicon wafers. The devices were peeled off the mold, cut, cleaned, and bonded to a glass slide precoated with a thin layer of PDMS following activation of both surfaces in an oxygen plasma (PDC 32G, Harrick) for 35 s. Polymer tubings (Upchurch Scientific) were inserted in the inlet and outlet holes and glued in place. The relevant microchannel dimensions are width $w = 300\,\mu$m, height $h \sim 130\,\mu$m, and channel length $L \sim 0.34$ m long. A meandering section is provided downstream of the inlet and comprises of 23 interconnected semi-circles starting at a downstream distance of $x = 12$ mm. The center-to-center distance between the semi-circles in the meandering section is ~1.4 mm (scaled figure provided in Fig. S1 of the supplementary material).[30]

C. Microfluidic device setup and operation

We dispensed aqueous mixtures of PEG and DEX as droplets carried by an immiscible fluorinated oil (FO) at a microfluidic T-junction and used high-speed optical microscopic imaging (Basler) to observe dynamic phase behavior (Fig. 1). Syringe pumps (Harvard, PHD 2000) were used to deliver FO (1:10 v/v mixture of perfluorooctanol and octadecafluorodecahydronaphthalene), a solution containing PEG, and another solution containing DEX to the microfluidic device. The

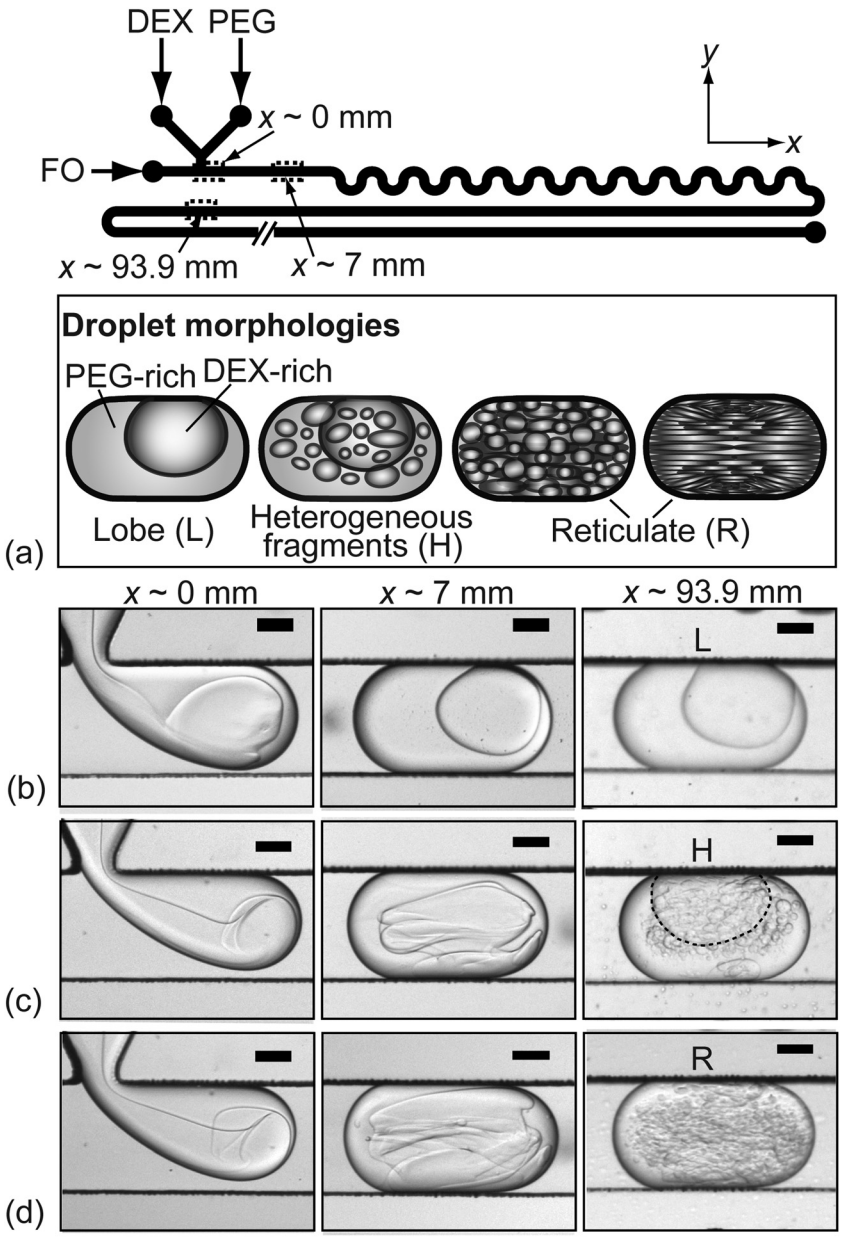

FIG. 1. (a) Schematic representation of device operation. Stereomicroscopic images of ATPS droplet structures ($C_{DEX} = 4.5\%$ w/w and $C_{PEG} = 5.0\%$ w/w) captured at various locations of the microchannels with increasing flow speeds, (b) 0.64 mm/s, (c) 4.3 mm/s, and (d) 7.5 mm/s. Scale bars represent 100 μm (enhanced online). (b) [URL: http://dx.doi.org/10.1063/1.3694841.1], (c) [URL: http://dx.doi.org/10.1063/1.3694841.2], (d) [URL: http://dx.doi.org/10.1063/1.3694841.3]

volumetric flow rate ratio of individual aqueous streams, Q_{PEG}:Q_{DEX}, was maintained at 1:1, while that of FO to total aqueous flow rate, Q_{FO}:($Q_{PEG} + Q_{DEX}$), was maintained at 1.5:1. In addition, various compositions (measured in wt. %) of PEG in the inlet PEG stream and DEX in the inlet DEX stream were used for the experiments. The compositions, C_{PEG} and C_{DEX}, mentioned hereafter, therefore, refer to the inlet stream compositions (wt. %) of PEG and DEX, respectively.

III. RESULTS AND DISCUSSION

At all compositions used in our experiments, the equilibrium case corresponds to droplets containing two *immiscible* aqueous phases: a PEG-rich outer phase encapsulating a DEX-rich

inner phase, with very low interfacial tension between phases.[3,4] Phase separation in mixtures of polymer solutions can be attributed to a less favorable entropy of mixing of long polymer chains and repulsive enthalpic interactions between the monomer units on the different polymers.[2] The thermodynamic state of this system can be influenced by polymer concentrations, molecular weight, temperature, and presence of inorganic salts.[2] The situation is different for moving droplets: a near continuum of speed and composition-dependent *non-equilibrium* phase morphologies is obtained (Fig. 1), ranging from the near-equilibrium drop-in-drop or lobe morphology (labeled as "L" in Fig. 1(b) (enhanced online)) to heterogeneous fragments (labeled as "H" in Fig. 1(c) (enhanced online)) and complex reticulate morphologies (labeled as "R" in Fig. 1(d) (enhanced online)). At low flow speeds, the ATPS droplets contain an intact DEX-rich drop encapsulated within the PEG-rich phase as shown in Fig. 1(b). As the flow speed increases, the inner DEX-rich phase is "stirred" within the outer PEG-rich phase. The DEX-rich phase deforms and eventually breaks up into a steady-state dispersion of heterogeneously sized drops (Fig. 1(c)), where the original large blob of DEX-rich phase coexists with smaller sized DEX-rich fragments. At even higher flow speeds, the ATPS droplets exhibit a reticulate structure, where DEX-rich phase is quite uniformly distributed in the PEG-rich phase as shown in Fig. 1(d). In this case, the DEX-rich phase may exist either as networks of extended filaments or as a dispersion of small drops or threads in the PEG-rich outer phase (see Fig. S2 in supplementary material for more images).[30]

The formation of these ATPS droplet structures is due to the competition between the interfacial tension (between PEG-rich phase and DEX-rich phase) and shear stress in the ATPS droplets, which can be characterized by a capillary number, $Ca = U\eta_c/\sigma$ (where U is the flow speed, η_c is the viscosity of the PEG-rich phase, and σ is the interfacial tension between PEG and DEX).[22,23,25] Increasing compositions lead to increase in interfacial tension[3,4] and viscosities of each phase. We measured the viscosities of the PEG-rich (η_c) and DEX-rich (η_d) phases for the range of compositions used in our experiments; both phases were found to be Newtonian and the viscosity ratio ($p = \eta_d/\eta_c$) ranges from ~5 to 61 (see Fig. S3 in supplementary material for interfacial tension data and viscosity measurements).[30] We map the influence of flow speed (U), and polymer composition (C_{PEG} *and* C_{DEX}) and construct a dynamic morphology diagram as shown in Fig. 2. Miscible ranges of PEG and DEX mixtures under static conditions are represented by the light grey region, while the dark grey region bounded by the black line marks conditions where the fluids yielded a parallel "co-flow" regime instead of forming ATPS droplets. Above the light grey region, the PEG and DEX mixture partitions into two visually distinct thermodynamic phases.

The transitions between the different regions on the map may be understood by invoking an analogy with simple models of drop dynamics in unconfined linear Stokes flow.[22–26] In our case, these models translate to the dynamics of a DEX-rich drop suspended in a PEG-rich external fluid in linear Stokes flow. In such models, it is well known that a critical capillary number Ca_c exists such that the DEX-rich drop remains stable when $Ca < Ca_c$ and deforms and breaks up when $Ca > Ca_c$; where Ca_c depends on the viscosity ratio and flow type.[22–26,31] Remarkably, in our experiments, the transition from lobe to heterogeneously fragmented morphologies is well fit by a critical capillary number of 0.15, which also agrees well with previous studies in the above model systems.[22,23,26] At low flow speeds where $Ca < Ca_c$, the interfacial tension dominates over the shear stress and its natural tendency to minimize the surface area results in the drop-in-drop morphology as in the static case. As the flow speed increases and the critical capillary number Ca_c is approached, the shear stress can now overcome the interfacial tension. The critical flow speed U_c required to provide the minimum shear stress to deform and breakup the DEX-rich phase for the polymeric mixtures of various composition is by definition $U_c = Ca_c \cdot \sigma/\eta_c$. From Fig. 2, U_c calculated from a constant $Ca_c \sim 0.15$ is seen to closely follow the measured boundary between lobe and heterogeneous fragment morphologies (curve I in Fig. 2), a remarkable conclusion considering the simplicity of the physical argument employed. At even higher flow speeds where the shear stress greatly exceeds the interfacial tension, the case now resembles the kinematic mixing of non-diffusing fluids within confined cavities.[32] At $Ca/Ca_c > 4$ (refer to curve II in Fig. 2 which indicates $Ca/Ca_c = 4$), we observe the emergence of reticulate network-like internal structures. The meandering microchannels in

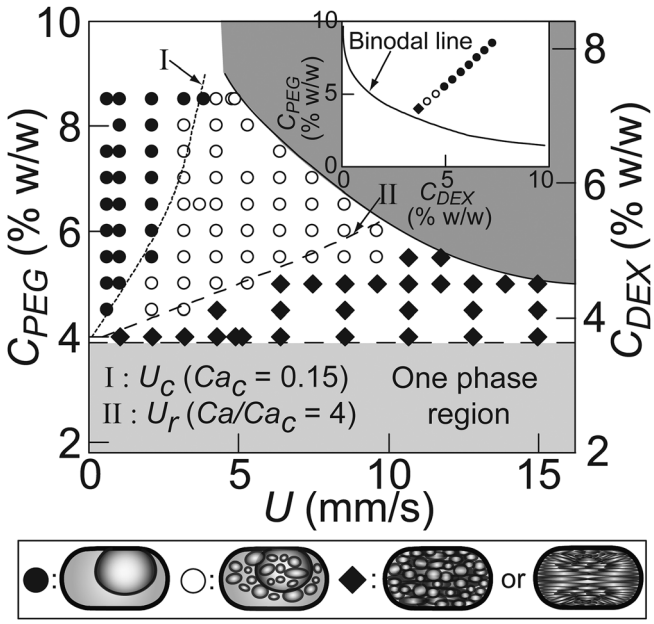

FIG. 2. Morphology map showing how flow speeds, U, and various compositions of PEG and DEX mixtures, C_{PEG} *and* C_{DEX}, influence structures of ATPS droplets. The inlet stream compositions of PEG (C_{PEG}) can be read from the left axis and the inlet stream compositions of DEX (C_{DEX}) can be read from the right axis. For instance, the close circle (●) on the top left of the morphology map refers to lobe morphology generated at $U = 0.64$ mm/s, $C_{DEX} = 7.3\%$ w/w, and $C_{PEG} = 8.5\%$ w/w. U_c is calculated using $Ca_c = 0.15$ and U_r is calculated using $Ca/Ca_c = 4$. The dark grey region bounded by the black line marks conditions where the fluids co-flow instead of forming ATPS droplets. The light grey area represents miscible compositions of PEG and DEX mixtures. Inset shows morphology behavior of PEG and DEX mixtures at flow speed of 2.1 mm/s, binodal line data are obtained from Diamond and Hsu (1989).[38]

our device provide time-dependent periodic stretching and folding of fluid interfaces, leading to chaotic advection of the DEX-rich phase within the PEG-rich phase, similar to that described in the context of miscible fluid mixing.[28] The inner DEX-rich phase is continually stretched, reoriented and folded, and ultimately exists either as uniformly dispersed networks of extended filaments or as a spatially uniform dispersion of small drops in the PEG-rich outer phase (Fig. 3(c) (enhanced online)).[28,33]

Digital analysis of high-resolution droplet images via the fast Fourier transform (FFT) technique, implemented in MATLAB (Mathworks, Inc.), enables us to extract characteristic sizes of these dispersed fluid elements (Fig. 4) (also see Fig. S2 in the supplementary material for more FFT images).[30] The measured characteristic lengths D_f, corresponding to the dominant intensity peaks in the direction transverse to flow are plotted against the flow speeds as shown in Fig. 4(d) and are observed to decrease with increasing flow speed. In the spirit of the above analysis, we compare these measured sizes with estimates for the diameters of viscous fluid filaments stretched in simple linear elongational flows. It is possible to calculate a critical thread diameter "D_{crit}" characterizing the minimum filament diameter before surface tension-driven breakup by estimating the maximum elongation rate ($\dot{\varepsilon}$) in the droplet as $\dot{\varepsilon} \sim U/h$.[24,26,27] (See supplementary material for detailed discussion of calculation procedure).[30] The diameter D_{crit} thus calculated corresponds to the finest possible filaments inside droplets. The calculated sizes (Fig. 4(d)) indeed decrease with increasing flow speed U. However, these theoretical estimates are still well below the measured D_f from FFT analysis. This is not entirely surprising considering the complexity of the actual flow situation in the drop—stretching filaments actively influence the overall flow field (which need not be linear), and filament folding and drop coalescence occur concurrently with stretching.[24,34]

The ATPS used in our work are typically characterized by low interfacial tensions and very diffuse fluid-fluid interfaces. Therefore, we compare the estimated filament size from FFT analysis with the thickness of the interface between the PEG-rich and DEX-rich phases. The

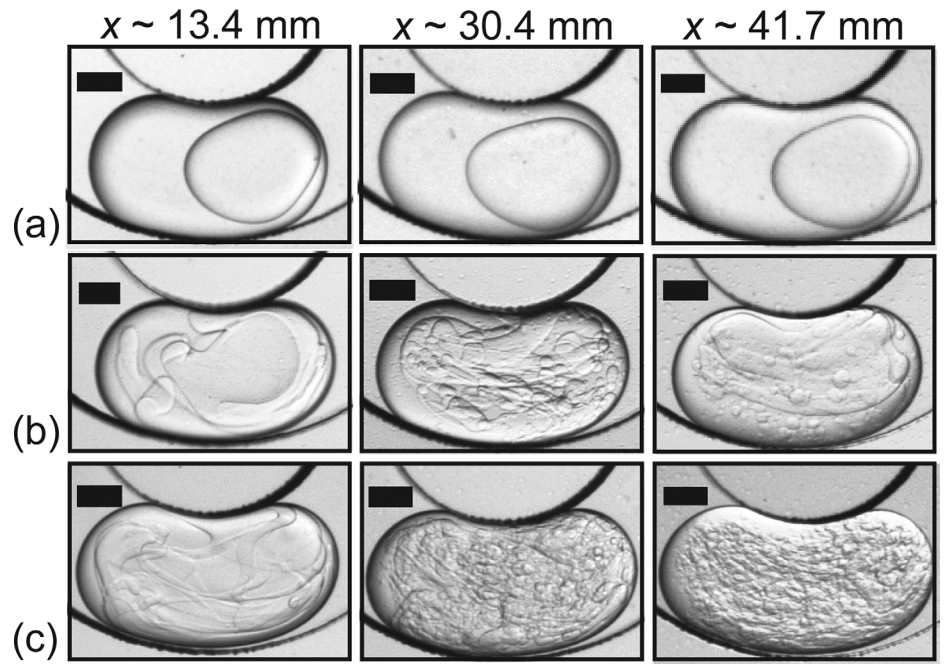

FIG. 3. Stereomicroscopic images of ATPS droplet structures ($C_{DEX} = 4.5\%$ w/w and $C_{PEG} = 5.0\%$ w/w) obtained along the meandering portion of the microchannel with increasing values of flow speeds (a) 0.64 mm/s, (b) 4.3 mm/s, and (c) 7.5 mm/s. Scale bars represent 100 μm (enhanced online). (b) [URL: http://dx.doi.org/10.1063/1.3694841.4], (c) [URL: http://dx.doi.org/10.1063/1.3694841.5]

equilibrium interface thickness in our system can be calculated using a modified Cahn-Hilliard formulation[35,36] where the interfacial tension is given by the following expression:

$$\sigma = \int_{-\infty}^{+\infty} \left(\Delta g(\phi_1, \phi_2) + \frac{K_1}{2} \left(\frac{d\phi_1}{dx} \right)^2 + K_{12} \left(\frac{d\phi_1}{dx} \right) \left(\frac{d\phi_2}{dx} \right) + \frac{K_2}{2} \left(\frac{d\phi_2}{dx} \right)^2 \right) dx,$$

where 1, 2, and 3 denote PEG, DEX, and water and ϕ_1, ϕ_2, and ϕ_3 are the volume fractions of PEG, DEX, and water, respectively; $g(\phi_1, \phi_2)$ represents the free energy of a uniform mixture of composition (ϕ_1, ϕ_2, 1-ϕ_1-ϕ_2), and K represents gradient energy parameters (K_1, K_2, K_{12}). By assuming that the interfacial compositions vary as a hypertangent function and using the experimental data for interfacial tension from Ryden and Albertsson,[3] we find that the interfacial thickness can be of the order of a few micrometers (See supplementary material for detailed calculation).[30] Indeed, the characteristic filament size does approach the order of interfacial thickness as can be seen from the analysis of the $C_{DEX} = 3.7\%$ w/w and $C_{PEG} = 4.0\%$ w/w mixture (Fig. 4(d)), which shows that the filament thickness can approach a few microns. This raises intriguing possibilities where biochemical reactions could be conducted in a diffuse, pseudo-homogeneous environment, and subsequently phase separated by simply reducing flow speed or widening the channel dimensions or by operating in "stop-start" fashion, as depicted in Fig. 5.

IV. CONCLUSION

Our work demonstrates the creation of droplets with tunable spatial heterogeneity in structure and composition, with potential applications in practical biochemistry as better *in vitro* analogues for the complex, crowded, and heterogeneous *in vivo* cellular milieus typical to most natural biochemistry.[6,37] Recent progress in biochemistry reveals that the biological cell is a rather complex heterogeneous environment, with an abundance of "soft interfaces," and where molecular crowding and confinement can profoundly affect the outcomes of biochemical processes.[37] Keeping this in view, the non-equilibrium "reticulate" structures are very interesting from the standpoint of practical biochemistry—these offer spatially structured, non-homogeneous, and

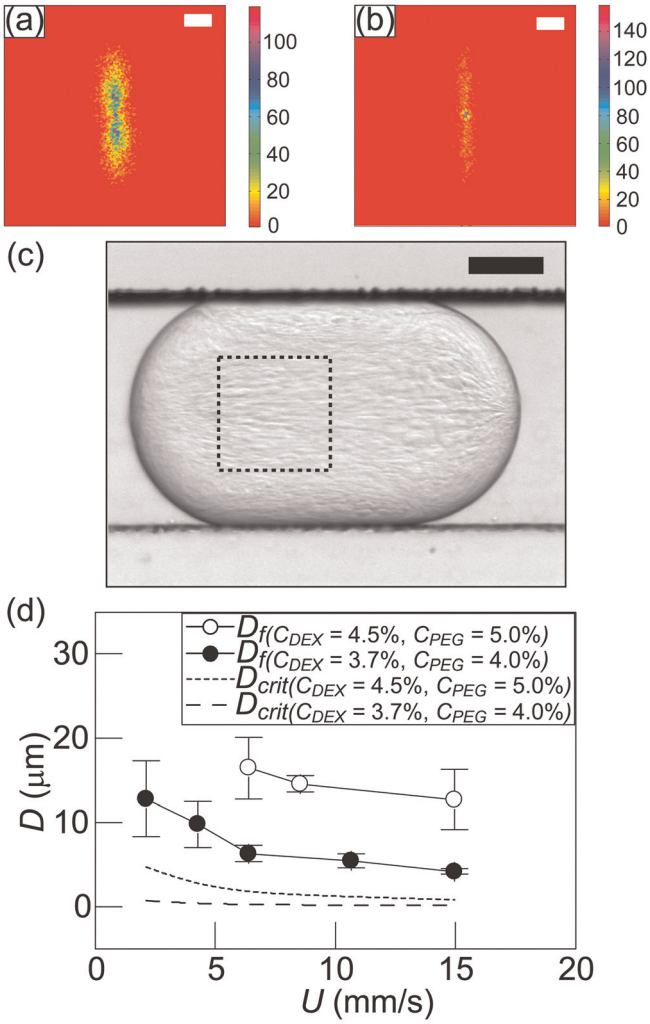

FIG. 4. 2D fast Fourier transform (FFT) analysis of flow images corresponding to (a) 2.1 mm/s and (b) 15.0 mm/s. Scale bars represent characteristic frequency, $f = 20$. (c) Stereomicroscopic image of a reticulate structure within an ATPS droplet ($C_{DEX} = 3.7\%$ w/w and $C_{PEG} = 4.0\%$ w/w) captured at $x \sim 93.9$ mm with a flow speed of 2.1 mm/s. Scale bar represents 100 μm. Dotted box indicates the area selected for FFT. (d) Characteristic size of reticulate filaments transverse to the principal flow direction, D_f ($C_{DEX} = 3.7\%$ w/w, $C_{PEG} = 4.0\%$ w/w and $C_{DEX} = 4.5\%$ w/w, $C_{PEG} = 5.0\%$ w/w), obtained from FFT with varying flow speeds, U. D_{crit} represents calculated filament size.

transient all-aqueous chemical environments comprised by thin (micron-scale) filaments of one fluid phase dispersed in the other and separated by soft, diffuse interfaces. Moreover, the presence of polymers in the "background" fluid environment can act to reinforce macromolecular crowding phenomena. Therefore, such droplets can potentially enable systematic interrogation of intriguing and novel questions about the role of the physical environment on the outcome of

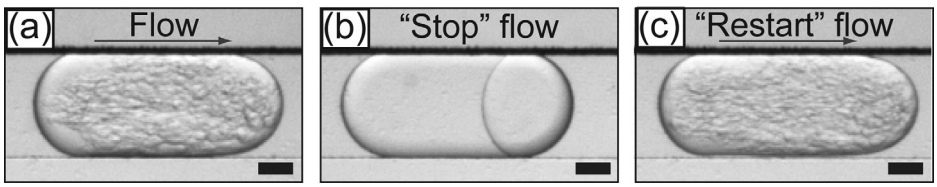

FIG. 5. Stereomicroscopic images captured at $x \sim 213$ mm (a) flowing ATPS droplet ($C_{DEX} = 5.0\%$ w/w and $C_{PEG} = 5.5\%$ w/w), (b) morphology change of ATPS droplet when flow is "stopped," and (c) morphology of droplet after flow is "restarted." Scale bars represent 100 μm.

biochemical reactions; for example—how does transient confinement of reactive biomolecules in thin fluid filaments with an abundance of soft fluid interfaces affect biochemical reaction rates? Is heterogeneous enzymatic catalysis at soft-interfaces possible? There is certainly a strong physical basis for these questions as biomolecular reaction rates depend on local species concentrations and biomolecular conformation, both of which are profoundly affected by the fluid environment. We also note that such investigations, while relevant, are challenging to undertake with conventional "macroscale" *in vitro* biochemical methods, which typically involve dilute aqueous solutions and do not capture the inherent *in vivo* chemical and morphological complexity.

ACKNOWLEDGMENTS

The authors would like to acknowledge funding from NUS Grant R-279-000-220-112/133 and the Chemical and Pharmaceutical Engineering Programme (CPE) of the Singapore-MIT Alliance.

[1]Y. S. Song, Y. H. Choi, and D. H. Kim, J. Chromatogr. A **1162**, 180 (2007).
[2]B. Y. Zaslavsky, *Aqueous Two-Phase Partitioning - Physical Chemistry and Bioanalytical Applications* (Marcel Dekker, New York, 1995).
[3]J. Ryden and P. A. Albertsson, J. Colloid. Interface Sci. **37**, 219 (1971).
[4]M. R. Helfrich, M. El-Kouedi, M. R. Etherton, and C. D. Keating, Langmuir **21**, 8478 (2005).
[5]F. Tjerneld and H. O. Johansson, Int. Rev. Cytol. **192**, 137 (2000).
[6]M. S. Long, C. D. Jones, M. R. Helfrich, L. K. Mangeney-Slavin, and C. D. Keating, Proc. Natl. Acad. Sci. U.S.A. **102**, 5920 (2005).
[7]I. Ziemecka, V. van Steijn, G. J. M. Koper, M. Rosso, A. M. Brizard, J. H. van Esch, and M. T. Kreutzer, Lab Chip **11**, 620 (2011).
[8]H. Tavana, A. Jovic, B. Mosadegh, Q. Y. Lee, X. Liu, K. E. Luker, G. D. Luker, S. J. Weiss, and S. Takayama, Nature Mater. **8**, 736 (2009).
[9]M. Yamada, V. Kasim, M. Nakashima, J. Edahiro, and M. Seki, Biotechnol. Bioeng. **88**, 489 (2004).
[10]K. H. Nam, W. J. Chang, H. Hong, S. M. Lim, D. I. Kim, and Y. M. Koo, Biomed. Microdevices **7**, 189 (2005).
[11]J. R. SooHoo and G. M. Walker, Biomed. Microdevices **11**, 323 (2009).
[12]M. Tsukamoto, S. Taira, S. Yamamura, Y. Morita, N. Nagatani, Y. Takamura, and E. Tamiya, Analyst **134**, 1994 (2009).
[13]K. Vijayakumar, S. Gulati, A. J. deMello, and J. B. Edel, Chem. Sci. **1**, 447 (2010).
[14]R. J. Meagher, Y. K. Light, and A. K. Singh, Lab Chip **8**, 527 (2008).
[15]G. Munchow, S. Hardt, J. P. Kutter, and K. S. Drese, Lab Chip **7**, 98 (2007).
[16]I. Ziemecka, V. van Steijn, G. J. M. Koper, M. T. Kreutzer, and J. H. van Esch, Soft Matter **7**, 9878 (2011).
[17]A. S. Utada, E. Lorenceau, D. R. Link, P. D. Kaplan, H. A. Stone, and D. A. Weitz, Science **308**, 537 (2005).
[18]S. Torza and S. G. Mason, J. Colloid. Interface Sci. **33**, 67 (1970).
[19]J. M. Ottino, *The Kinematics of Mixing: Stretching, Chaos, and Transport* (Cambridge University Press, UK, 1989).
[20]J. M. Ottino, Sci. Am. **260**, 56 (1989).
[21]C. J. Allegre and D. L. Turcotte, Nature **323**, 123 (1986).
[22]B. J. Bentley and L. G. Leal, J. Fluid Mech. **167**, 241 (1986).
[23]H. P. Grace, Chem. Eng. Commun. **14**, 225 (1982).
[24]J. M. H. Janssen and H. E. H. Meijer, J. Rheol. **37**, 597 (1993).
[25]G. I. Taylor, Proc. R. Soc. London, Ser. A **146**, 501 (1934).
[26]J. M. H. Janssen, "Dynamics of liquid-liquid mixing," Ph.D. dissertation (Eindhoven University of Technology, 1993).
[27]D. V. Khakhar and J. M. Ottino, Int. J. Multiphase Flow **13**, 71 (1987).
[28]M. R. Bringer, C. J. Gerdts, H. Song, J. D. Tice, and R. F. Ismagilov, Phil. Trans. R. Soc. London, Ser. A **362**, 1087 (2004).
[29]Y. Xia and G. M. Whitesides, Annu. Rev. Mater. Sci. **28**, 153 (1998).
[30]See supplementary material at http://dx.doi.org/10.1063/1.3694841 for a scaled version of the actual channel pattern, more images of reticulate structures, interfacial tension and viscosity data, detailed calculation of D_{crit}, and detailed discussion of calculation of interfacial thickness.
[31]D. V. Khakhar and J. M. Ottino, J. Fluid Mech. **166**, 265 (1986).
[32]R. Chella and J. M. Ottino, Ind. Eng. Chem. Fundam. **24**, 170 (1985).
[33]S. Y. Teh, R. Lin, L. H. Hung, and A. P. Lee, Lab Chip **8**, 198 (2008).
[34]M. Tjahjadi and J. M. Ottino, J. Fluid Mech. **232**, 191 (1991).
[35]J. W. Cahn and J. E. Hilliard, J. Chem. Phys. **28**, 258 (1958).
[36]D. Q. He, S. Kwak, and E. B. Nauman, Macromol. Theory Simul. **5**, 801 (1996).
[37]R. J. Ellis and A. P. Minton, Nature **425**, 27 (2003).
[38]A. D. Diamond and J. T. Hsu, Biotechnol. Tech. **3**, 119 (1989).